Hydrogen-induced magnetization and tunable hydrogen storage in graphitic structures

Yang Lei, Stephen A. Shevlin, Wenguang Zhu,* and Zheng Xiao Guo†
Department of Chemistry, University College London, London WC1H 0AJ, United Kingdom
(Received 27 June 2007; published 24 April 2008)

Hydrogen interactions with undefective and defective graphitic structures were investigated by first-principles simulations. Structural vacancies were identified to promote the dissociation of molecular hydrogen with a reduced activation barrier of 0.63 eV, compared to 2.38 eV for a perfect graphene. However, the vacancies bind the hydrogen too strongly for spill-over mechanisms to be effective. An isolated vacancy in a graphene can bind four hydrogen atoms, but a metastable and magnetic structure binds six hydrogen atoms at the vacancy site at room temperature. The thermodynamics, magnetic properties, and hydrogen binding energies vary with graphene layer spacing. A metastable structure becomes energetically favorable for a layer spacing of 3.19 Å, while the binding of hydrogen becomes exothermic at a layer spacing of 2.72 Å. This phenomenon suggests the possibility of using hydrogen-rich carbon structures for reversible magnetic and hydrogen storage applications.

DOI: 10.1103/PhysRevB.77.134114 PACS number(s): 81.05.Uw, 68.43.−h, 73.22.−f

I. INTRODUCTION

There is a global drive in developing clean and renewable energy sources due to CO_2-exacerbated climate change, depletion of fossil fuels, and vehicle-related air pollution.[1,2] Hydrogen is a clean energy carrier for thermal or cold combustion. However, one of the main issues limiting its use is the difficulty of storage. Atomic hydrogen storage in a solid, e.g., a hydride, provides a relatively safe and practical choice and can have a relatively large volumetric capacity.[3] An ideal storage material for hydrogen should possess a high capacity, a low dissociation temperature (<150 °C) under moderate pressures, high kinetics for H sorption, lightweight, high cyclability, and stability against O_2 and moisture. Different types of materials have been studied, including $LaNi_5$ alloys,[4] TiFe compounds,[5] Zr- and Ti-based Laves phases,[6] and Mg_2Ni and Mg based materials,[7] amides, and complexes (sodium alanate related hydrides[8]). Unfortunately, none of these satisfy all the essential requirements.

Carbon nanostructures are also strong candidates for hydrogen storage, with early reports of H_2 uptake around 7.4 wt % in nanostructured graphite[9] and 14 wt % in single wall carbon nanotubes (SWNTs).[10] More credible reports indicate that hydrogen adsorption in graphite nanofibers (3.8 wt %) (Ref. 11) and SWNTs (5.1 ± 1.2 wt %) (Ref. 12) exceed the limit of room temperature physisorption (1 wt %).[13] However, the exact mechanisms for this relatively high hydrogen uptake are unclear.

Several first-principles density functional theory (DFT) studies have been performed on carbon nanostructures in order to explain the reported variations in hydrogen storage capacity.[10,14–20] Lee and Lee showed that more than 14.3 wt % hydrogen can be stored in pure SWNTs using a tight-binding approach, with coexisting exothermic chemisorption and endothermic physisorption.[14] In addition, recent *ab initio* calculations predict more than 7 wt % hydrogen uptake by SWNTs[19] and ~9 wt % in fullerenes but only with the addition of transition-metal atom decorants.[20] However, these attempts have not explained the experimentally reported capacity differences in a given carbon nanostructure. It is noted that most of the theoretical papers concentrate on perfect nanostructures. Realistic carbon nanostructures always possess various kinds of defects, for example, dangling bonds at open ends, vacancies, or other structural defects,[21–26] as observed by transmission electron microscopy.[27] Such defects can lead to considerable differences in hydrogen uptake and may hold the key to unlocking the principle mechanisms of varied hydrogen storage in carbon nanostructures.

Here, we use first-principles simulations to investigate the interactions between hydrogen and graphitic structures, with and without vacancies. The stable adsorption sites of atomic and molecular hydrogen on single graphene sheets and in bulk graphite were compared, as well as the barrier energies for hydrogen diffusion and dissociation on defective and undefective systems. The effects of vacancy and interlayer spacing on hydrogen adsorption were investigated. The storage capacity at a vacancy increases with decreasing interlayer spacing, indicating a mechanism for tunable hydrogen storage. In addition, an unusual and unexpected magnetic ground state was discovered when the interlayer spacing is reduced in the presence of hydrogen, which may be of interest to magnetic applications.

II. METHODOLOGY

DFT simulations were performed using the Vienna ab initio simulation package (VASP).[28,29] Ultrasoft pseudopotentials[30] were used to treat the core electrons. The size of the supercell of a single graphene sheet is $4\sqrt{3}d \times 6d \times c$ [where, based on our calculations, d is set to the theoretical lattice parameter 1.42 Å, very close to the experimental value of 1.421 Å (Ref. 31)]. The vacuum thickness c is set to 10.0 Å. For the bulk, we consider two graphene layers with the interlayer distance set to the theoretical lattice parameter of 3.32 Å [close to the experimental value of 3.35 Å (Ref. 31)]. A single graphite layer with a vacancy density of 3.2% and a two-layer bulk graphite supercell with a 1.6% vacancy density were investigated (see Fig. 1). Several calculations were checked, however, by run-

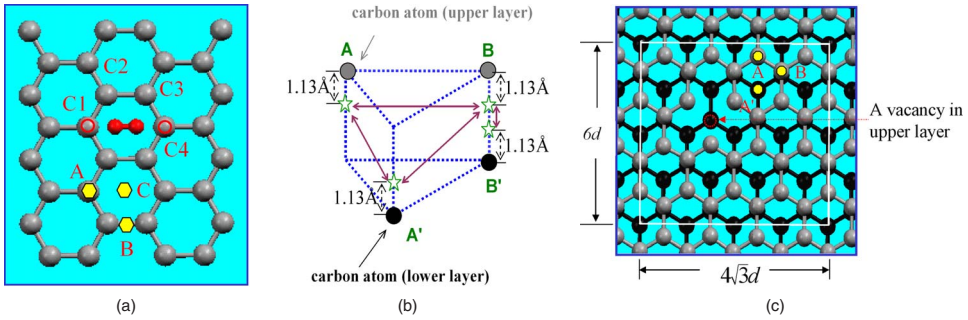

FIG. 1. (Color online) Schematic of (a) hydrogen adsorption sites (yellow hexagon) on a graphene sheet and structures before (solid circle) and after (open circle) H_2 dissociation, (b) bulk graphite with vacancy and adsorption sites (yellow hexagon), and (c) possible diffusion paths for hydrogen atoms in bulk graphite.

ning four layer simulations, with no significant change in results. A plane wave basis set was used with a kinetic energy cutoff of 287 eV. The Brillouin zone was sampled using the Monkhorst-Pack scheme[32] with a (221) mesh. All atoms were fully relaxed until the change in force upon ionic displacement was less than 0.03 eV/Å. We used the local density approximation (LDA) treatment for exchange and correlation as it more accurately describes the weak molecular H_2-carbon interaction,[33,34] although the generalized gradient approximation (GGA) was used to check several results. All calculations are spin polarized. The nudged elastic band (NEB) method[35] was used to determine energy barriers.

III. RESULTS

A. Hydrogen interaction with a perfect graphene sheet

For the adsorption of a single H atom on graphene, there are three possible adsorption sites: *A* (over a carbon atom), *B* (over a C-C bridge), and *C* (over the center of the hexagon) [Fig. 1(a)]. We identified that the most stable position for a H atom is on the top of a carbon atom, the *A* site. The binding energies of a single H atom and a H_2 molecule adsorbed on the graphene sheet are defined, respectively, as follows:

$$E_b = E_{(G+\mathrm{H})} - E_G - \frac{1}{2}E_{\mathrm{H}_2},$$

$$E_b = E_{(G+\mathrm{H}_2)} - E_G - E_{\mathrm{H}_2}, \quad (1)$$

where E_G is the total energy of the relaxed graphene sheet, E_{H_2} is the energy of an isolated hydrogen molecule in free space, $E_{(G+\mathrm{H})}$ and $E_{(G+\mathrm{H}_2)}$ are the total energies of the relaxed graphene sheet upon single hydrogen and molecular hydrogen adsorption, respectively. A more negative E_b indicates a stronger binding between the hydrogen and the carbon structures. We find that the binding energy and the length of the C-H bond for a single H atom are −1.32 eV and 1.13 Å, which agree with the binding energies of −1.30 to −1.40 eV (Ref. 36) and a length of 1.11 Å in the literature, respectively.[37] The chemisorption of a H atom induces sp^3 hybridization with a C atom, pulling the C atom out of the surface.

The binding energy of a hydrogen molecule on a graphene sheet was determined to be −0.10 eV regardless of adsorption site and orientation, in agreement with −0.09 eV found in early theoretical studies.[15,38] Typically, the adsorption energy is overestimated and the predicted equilibrium distance is too short from the results within the local density approximation.[39,40] Compared with the experimental value (0.04 eV) of the binding energy between H_2 and a graphitic surface,[41] our result (0.10 eV) shows an overestimation. The H_2 molecule resides in the center of the hexagon. The physisorption of the H_2 molecule is not sufficiently strong to change the geometry of the graphene sheet.

The energy barriers for a single H atom to diffuse from the *A* site to the *B* site and from the *A* site to the *C* site were calculated using the NEB method (Fig. 2). The *B* and *C* sites are not local minima but saddle points; only the *A* site is the stable adsorption site. The lowest energy diffusion pathway for a single hydrogen atom is from an *A* site to another neighboring *A* site via a *B* site, with a corresponding energy barrier of 1.19 eV [Fig. 2(a)], while the energy barrier is 1.84 eV for the alternative path of *A*-*C*-*A* [Fig. 2(b)]. This implies that the H atom prefers to move along the C-C bonds, rather than traverse above the hexagonal carbon rings.

The dissociation energy of a hydrogen molecule on a graphene sheet was calculated in order to determine the stable form of hydrogen sorption. A hydrogen molecule was respectively adsorbed at sites *A*, *B*, or *C* on the graphene sheet in the initial state (Fig. 1). In the final state, the H_2 molecule is dissociated to form two H atoms. There are three different adsorption sites for the hydrogen atoms after dissociation, $C1+C2$, $C1+C3$, and $C1+C4$ [Fig. 1(a)]. Out of these configurations, the minimum barrier energy was determined as 2.38 eV, on the $(C1+C4)$ site [Fig. 1(a)], which is

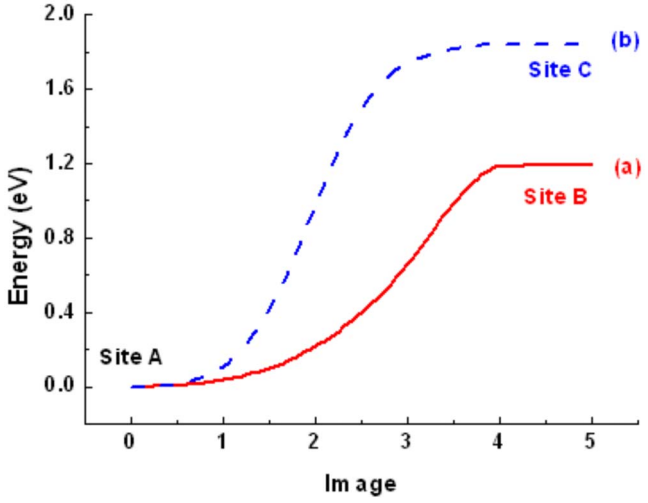

FIG. 2. (Color online) Minimum energy pathways of atomic H diffusion between different sites: (a) $A \rightarrow B$ and (b) $A \rightarrow C$.

less than the value reported by Miura *et al.* (a barrier of 3.3 eV for H_2 dissociation on a graphene sheet[42]). It is energetically favorable for hydrogen to adsorb in a molecular form than the dissociated form by 1.08 eV.

B. Bulk graphite

There are two nonequivalent stable sites for a single H atom to adsorb onto carbon atoms in bulk graphite (α or 2H phase, with *ABAB* stacking) [Fig. 1(b)]: site A corresponds to a carbon atom in one layer above the center of a hexagon of an adjacent layer, an "off-site" position, and site B corresponds to one carbon atom above another, an "on-site" position. The respective hydrogen binding energies for A and B were -1.23 and -1.09 eV, which implies that the carbon atoms in the neighboring layer affect the C-H binding. The H atom forms a strong bond with the carbon atom, with a bond length of 1.13 Å for both cases, similar to the situation when hydrogen is adsorbed on a single graphene sheet.

For atomic hydrogen diffusion in the graphitic structure, there are four adjacent positions, A, A', B, and B' (sites A and A' are equivalent, and B and B' are equivalent) [Fig. 1(c)], which provide six nonequivalent diffusion paths: $A \rightarrow B$, $B \rightarrow A$, $A' \rightarrow B$, $B \rightarrow A'$, $A \leftrightarrow A'$, and $B \leftrightarrow B'$. Only route $A \leftrightarrow B$ corresponds to hydrogen transport directly along a C-C bond in the same sheet, and the others involve hydrogen transport toward an adjacent sheet. When H atoms diffuse from B to B', the energy barrier is lower than that from A to A' because the C-H binding at site B is weaker than that at site A. Considering the barrier energies, the most energetically favorable step for the atomic transport of hydrogen is between two adjacent sheets with at least the starting or the end point at site B (or B'), i.e., between two on-site carbon atoms. With the barrier energies ranging from 0.42 ($B \leftrightarrow B'$), 0.48 ($B \rightarrow A'$), 0.64 ($A' \rightarrow B$), 0.81 ($A \leftrightarrow A'$), 0.94 ($B \rightarrow A$), to 1.09 ($A \rightarrow B$) eV, atomic transport of hydrogen is likely to occur along C-C bonds between two adjacent graphene layers in bulk graphite (Fig. 3).

C. Hydrogen interaction with graphene vacancy

Real carbon systems will be defective; therefore, we consider the interaction of an atomic vacancy with hydrogen. The formation energy of the vacancy, E_f, is defined as follows:

$$E_f = E_G - E_{GV} - E_C, \tag{2}$$

where E_G, E_{GV}, and E_C are the total energies of the perfect graphene sheet, the defective graphene sheet, and an isolated carbon atom in the free space, respectively. E_f is determined to be 8.00 eV in our calculations, similar to the values (7.0–8.0 eV) reported in the literature.[43–45]

When a single H atom is adsorbed on the carbon atoms around the vacancy, a strong C-H bond is formed. Our calculations show that the barrier energy for a single H atom to diffuse between two carbon atoms around the vacancy is 3.45 eV [see Fig. 4(a)]; three times that for a H atom to diffuse on the perfect graphene sheet. The vacancy binds the hydrogen very strongly (the binding energy is -2.1 eV). In contrast, the barrier for a single hydrogen atom to diffuse toward the vacancy is only 0.5 eV, which means that it is thermodynamically much easier for a single hydrogen atom to diffuse toward the vacancy than away from it. Hydrogen atoms chemisorbed on a graphene sheet will tend to diffuse toward a bare vacancy. However, these bind the hydrogen too strongly for spill-over mechanisms to be effective.

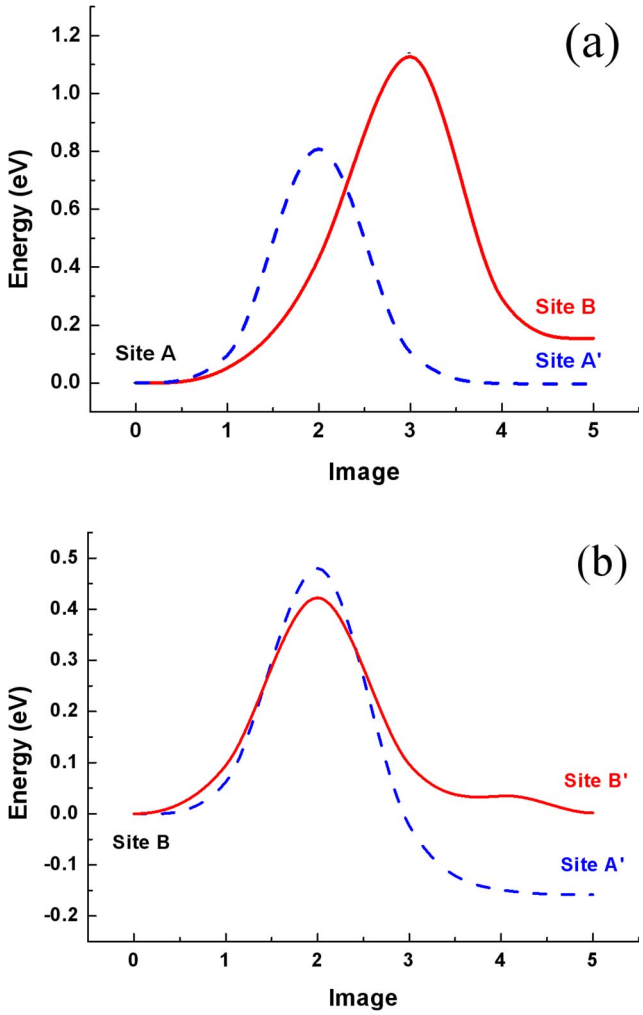

FIG. 3. (Color online) Minimum energy pathways for H atomic diffusion between (a) sites $A \leftrightarrow A'$ (dash line) and $A \leftrightarrow B$ (solid line) and (b) $B \leftrightarrow B'$ (solid line) and $B \leftrightarrow A'$ (dash line).

As mentioned above, the barrier energy for the dissociation of a H_2 molecule on a perfect graphene sheet is 2.38 eV. When a vacancy is present, the height of the barrier is greatly decreased to 0.63 eV (see Fig. 5). In contrast, it is very hard for the H atoms to recombine and form H_2, as the barrier energy for the reverse reaction is around 4 eV, which means that atomic hydrogen storage on a vacancy is very stable. The physisorption of a H_2 molecule on the vacancy gives a binding energy of 0.17 eV, whereas the calculated van der Waals correction is 0.018 eV. Hence, this correction to the thermodynamics is relatively small and can be neglected. This is not surprising: we consider systems where atomic bonds are formed with much stronger binding energies than H_2 physisorption and that are well described in DFT. These

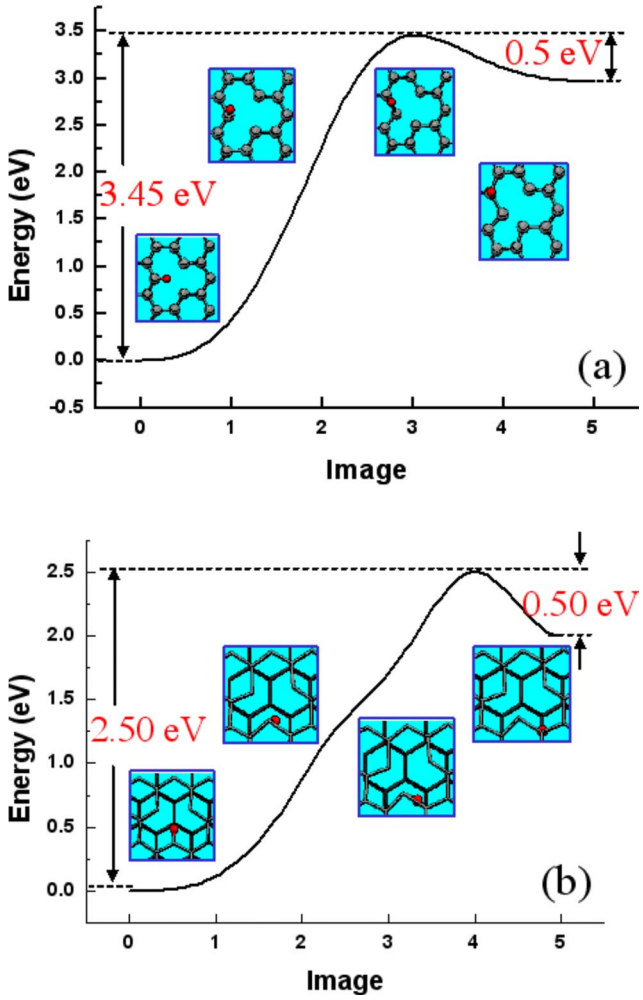

FIG. 4. (Color online) Minimum energy pathways for atomic H diffusion between two carbon atoms around the vacancy in (a) a single graphene sheet and in (b) bulk graphite.

atomic bonds will dominate the thermodynamics of the system.

To determine the maximum hydrogen storage capacity of a vacancy, more hydrogen was added to the system. We define the successive binding energy per H_2 molecule E_b as

$$E_b(\mathrm{H_2}) = E_{(G+n\mathrm{H_2})} - E_{[G+(n-1)\mathrm{H_2}]} - \frac{1}{2}E_{\mathrm{H_2}}, \quad \text{when } n \text{ is odd},$$

$$E_b(\mathrm{H_2}) = E_{(G+n\mathrm{H_2})} - E_{[G+(n-2)\mathrm{H_2}]} - E_{\mathrm{H_2}}, \quad \text{when } n \text{ is even}, \tag{3}$$

where E_G is the total energy of the optimized graphene sheet with a vacancy, $E_{\mathrm{H_2}}$ is the energy of an isolated hydrogen molecule, $E_{(G+n\mathrm{H_2})}$ is the energy of the optimized vacancy structure upon molecular hydrogen adsorption, and n is the number of hydrogen atoms in the supercell. The binding energies and structures of the hydrogenated vacancy (with one to six hydrogen atoms present) are shown in Fig. 6.

It is clear that the vacancy site can adsorb up to four H atoms with a binding energy per hydrogen molecule much

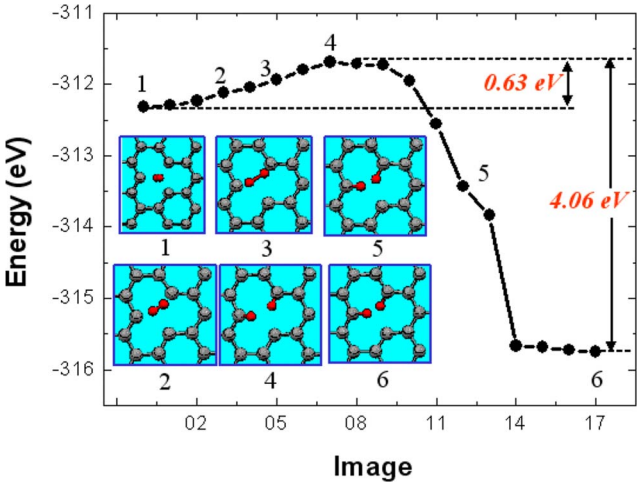

FIG. 5. (Color online) Minimum energy pathways for a single H_2 to dissociate on a vacancy in a single graphene sheet.

higher than that of H_2 binding to a perfect graphene sheet (−0.1 eV). On the other hand, E_b decreases in magnitude for the fifth and sixth H atoms, so that the binding is even weaker than for hydrogen adsorption on a perfect graphene sheet. This means that extra hydrogen does not prefer to be adsorbed at the vacancy site. In summary, addition of two H_2 molecules results in chemisorption to the carbon atoms neighboring the vacancy, but $3H_2$ addition results in a $4H+H_2$ structure. However, we note that when six H atoms are introduced to the system, there is a metastable structure, where two H atoms are bound to each exposed C atom at the vacancy for a maximum hydrogen sorption capacity of 6H with the carbon atoms strongly distorted from their sp^2 configuration. We found that the $4H+H_2$ structure has a lower total energy by 1.5 eV and thus is energetically favorable. Furthermore, our calculations show that the 6H structure has a magnetic moment of $1.9\mu_B$ but the $4H+H_2$ is nonmagnetic.

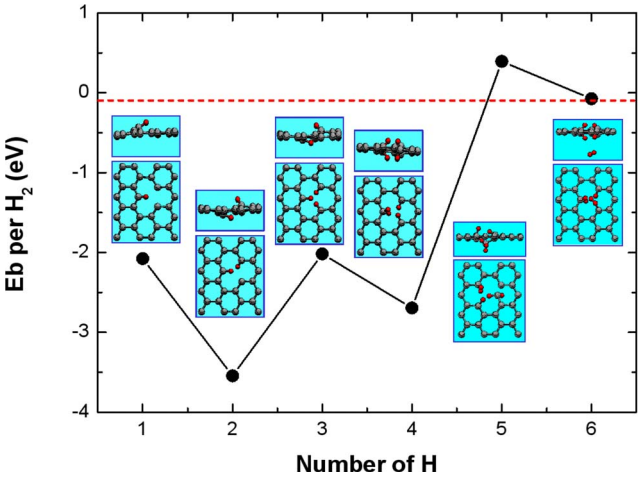

FIG. 6. (Color online) Adsorption energy E_b (per H_2) as a function of the number of hydrogen atoms (1–6) adsorbed at the vacancy site on a single graphene sheet. [Red dash line: E_b (per H_2) of one H_2 on a perfect graphene is −0.1 eV.]

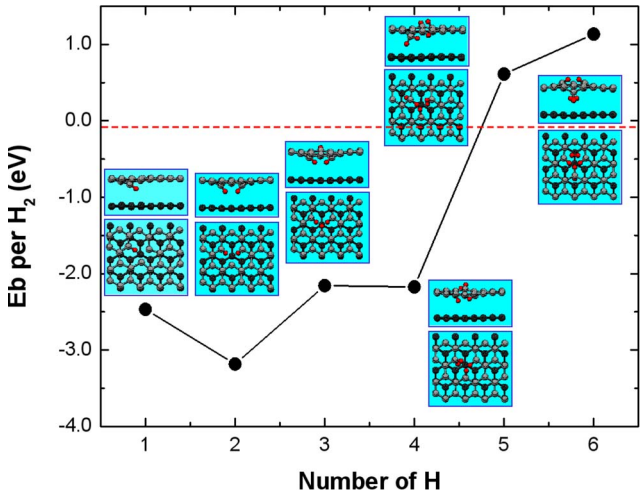

FIG. 7. (Color online) Adsorption energy E_b (per H_2) as a function of the number of hydrogen atoms (1–6) adsorbed around a vacancy in bulk graphite. [Red dash line: E_b (per H_2) of one H_2 on a perfect bulk graphite is −0.08 eV.]

D. Graphite with vacancy

We now consider the effects of multiple carbon layers on H passivation of a vacancy. The reaction path of a single H atom diffusing around the vacancy in bulk graphite was calculated [Fig. 4(b)]. A barrier of 2.5 eV has to be overcome for one H atom to diffuse between two adjacent carbon atoms near the vacancy, twice that of the energy needed for an atomic H to diffuse in undefective graphite. Thus, the H atom has a strong tendency to move toward the vacancy, rather than away from it, and the barrier energy for H diffusing into the vacancy is only 0.5 eV, the same as for the case with a single graphene sheet. However, the barrier energies for H diffusion away from a vacancy in a single graphene sheet and in bulk graphite are different by about 1 eV. This phenomenon may be explained by the image charge induced in neighboring perfect graphene sheets by the carbon-hydrogen bonding. Due to the difference in electronegativity, covalent bond formation involves electron density transfer from the H to the C atom. As a result, the carbon atom is negatively charged with respect to the unbound system, and the hydrogen atom is positively charged. This electric dipole induces an image dipole in the neighboring perfect graphene layers. This weakens the C-H binding, explaining the weaker C-H bonding when compared with the single graphene sheet. As a check, a four layer unit cell with a single atom vacancy on one graphene sheet was simulated. A determination of the charge density difference shows that the induced image dipole is localized on the graphene sheet next to the defective sheet. Therefore, two layers in the supercell are sufficiently accurate to model the dipole effect in bulk and the image interaction only happens on the perfect carbon layers adjacent to the defective layer.

Secondly, one to six H atoms are introduced into the system and the binding energy per H_2 and structure were determined (see Fig. 7). Similar to the single-sheet case, the bulk vacancy only adsorbs 4H. When a single H_2 molecule is inserted at the vacancy site of the bulk, it dissociates readily

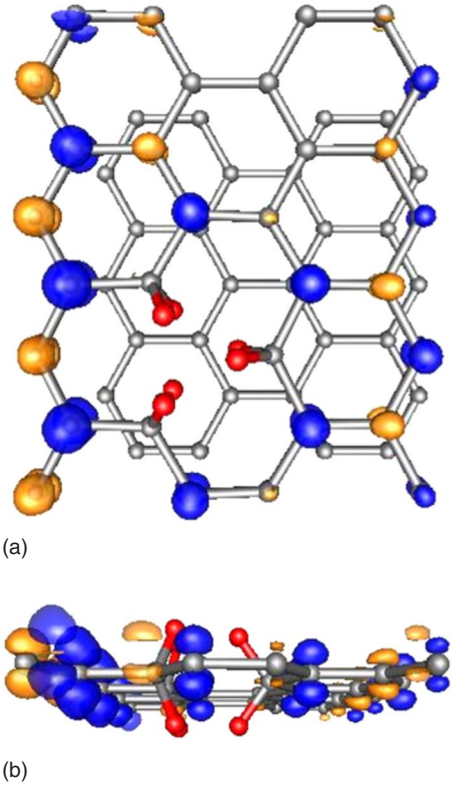

FIG. 8. (Color online) Spin-density plot for defective bulk graphite with 6H, with orange representing negative charge ($-0.001e$) and blue representing positive charge ($0.005e$): (a) top view and (b) side view.

and bonds with the carbons around the vacancy. When six H atoms are added, two possible configurations exist and, as for the single graphene sheet, the $4H+H_2$ structure is the ground state, while the 6H structure is metastable. The total energy of the $4H+H_2$ system is 0.63 eV lower than the 6H atoms adsorbed at the defective site. We also found that the former structure is nonmagnetic, but the latter possesses a magnetic moment of $0.08\mu_B$, much weaker than the case with the single graphene sheet. The van der Waals interaction between the sheets quenches the magnetization of the vacancy with respect to the isolated sheet. Comparison of the spin densities before and after 6H chemisorption shows that the formation of six σ bonds triggers delocalized π-electron spin polarization that is confined to the defective graphene sheet, as shown in a plot of the spin density (Fig. 8). The magnetic moment is, however, extremely small. Such a small difference in energy may result in DFT techniques erroneously ascribing a magnetic ground state to the system due to the errors in the pseudopotentials and the treatment of exchange correlation. We emphasize that we performed both LDA and GGA simulations of the 6H structure (both supercells using their theoretical lattice parameters) and found that this structure is magnetic. The only difference being that the GGA simulations showed a stronger magnetic moment for the bulk than the LDA. We ascribe this to the weaker interaction between sheets of the GGA functional. Our observation of magnetization in nanostructured carbon agrees with theory and experiment, where the adsorption of hydrogen on carbon

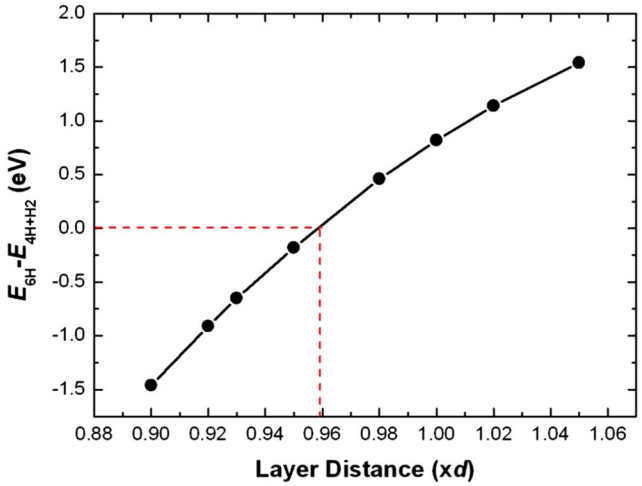

FIG. 9. (Color online) Energy difference between (B+6H) and (B+4H+H_2) when the layer distance between adjacent carbon sheets is changed slightly. Configuration "B" represents the defective bulk graphite. (The red dash shows the layer distance when the energy difference is zero.)

atoms at the edge of graphite[46–48] and on a vacancy of a SWNT introduces finite spin moments into the system.[49]

The difference in energy between the metastable 6H structure and the stable 4H+H_2 structure was determined as a function of layer spacing (see Fig. 9). We found that the 6H structure becomes stable for layer spacings less than 0.96d (d=equilibrium layer spacing), with the magnetization disappearing due to the increase in intrasheet interactions. The experimental value of the graphite bulk modulus is 28.6 GPa, which means that a pressure of 1.144 GPa is needed to reduce the layer distance to 96%.[50] Room temperature molecular dynamics calculations were performed to determine stability; after 1.5 ps of elapsed time, the metastable 6H structure was still stable. As shown in Fig. 10, the binding energy E_b per H_2 for the 6H structure becomes negative when the layer distance is squeezed to less than 82%. This indicates that it is energetically favorable for hydrogen to be adsorbed around the vacancy rather than persist in free space as a molecule. As presented in Fig. 10, additional hydrogenation energetics (the 4H to 6H hydrogenation) can be modified via compression of the interlayer spacing. Therefore, the binding energy can become negative and of magnitude of 0–1 eV, low enough for reversible hydrogen storage and appropriate for hydrogen storage applications.

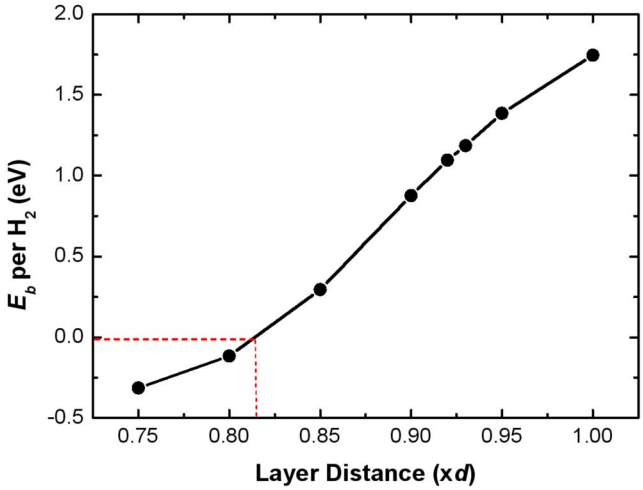

FIG. 10. (Color online) Binding energy per H_2 of the defective bulk with 6H as a function of layer distance. (The red dash line shows the layer distance when E_b=0.)

Our calculation is at zero temperature and, therefore, temperature effects are neglected. Thermodynamically, hydrogen adsorption is governed by the change in free energy $\Delta G=\Delta H-T\Delta S=\Delta E+p\Delta V-T\Delta S$, so that ΔG becomes negative,[51] where the symbols have their usual meanings. Trapping H_2 results in a decrease in the system entropy, which is dominated by the entropy of hydrogen gas S_{H_2}, with $-T\Delta S \approx TS_{H_2}$. Thus, this is a positive contribution. There is another term, $p\Delta V$, which can counteract this. When the bulk system is compressed, $p\Delta V$ becomes negative. At some point, the pressure contribution outweighs the entropy contribution, thus changing the sign of ΔG from positive to negative. Based on our calculations, we evaluate $p\Delta V$ to be −0.751 eV at the point when 4H+H_2 becomes energetically unfavorable with respect to the 6H structure (the layer distance compressed to 96%). This may be compared with the data in Ref. 52 where $-T\Delta S$ is 0.685 eV at 200 K at a pressure of 1 GPa. At this crossover point, the $p\Delta V$ term is large enough to counteract the entropy term and make the process exothermic at the specific compression conditions we are looking at. As the pressure is constant for small changes in ΔV at this compression, we find that the point at which the pressure term equals the entropy term is at a ΔV of 0.037. This means that the entropy effects are not important in the region of compression, where atomic hydrogen adsorption is around the vacancy in the ground state structure.

IV. CONCLUSIONS

We have investigated via first-principles simulation the interaction of hydrogen with both undefective and defective single graphene and bulk graphite systems. On ideal graphene sheets, hydrogen prefers to adsorb molecularly via weak physisorption, but on a carbon vacancy, hydrogen prefers to bind strongly in atomic form via chemisorption with a hydrogen dissociation barrier of 0.63 eV. Atomic hydrogen transport in bulk graphite was found to proceed via jumps between adjacent graphene sheets. Up to four hydrogen atoms can be bound on a vacancy, although we identify another metastable structure (compared to a 4H+H_2 structure) that binds six hydrogen atoms, which is itself stable at room temperature. This metastable structure is magnetic; however, the magnetism is quenched with reduced interlayer spacing. This reduction in interlayer spacing also changes the thermodynamics of the system: with decreasing layer spacing, the 6H system becomes energetically preferred at a pressure of 1.14 GPa, implying that nanostructured graphite can be reversibly switched between magnetic and nonmagnetic

states by pressure induced manipulation in the presence of hydrogen. With decreasing layer spacing, the adsorption of six hydrogen atoms on the vacancy also becomes exothermic with respect to free molecular hydrogen. This combination of hydrogen-induced magnetism and changeable thermodynamics upon variation of the graphene layer spacing implies the potential for nanostructured defective carbon-based nanostructures to act as a reversible magnetic system, as well as a tunable hydrogen storage material.

ACKNOWLEDGMENTS

The work was supported in part by the EPSRC UK Sustainable Hydrogen Energy Consortium (UK-SHEC), U.S. National Science Foundation (DMR-0306239 and DMR-0325218), and Oak Ridge National Laboratory, managed by UT-Battelle, LLC for the U.S. Department of Energy under Contract No. DE-AC05-00OR22725. Some of the calculations were performed at NERSC of DOE and CCS of ORNL.

*Also at Department of Physics, University of Texas, Austin, TX 78712 and Materials Science and Technology Division, Oak Ridge National Laboratory, TN 37831.

†Corresponding author; FAX: +44 20 7679 7527; z.x.guo@ucl.ac.uk

[1] U.S. DOE, Hydrogen Fuel Cells and Infrastructure Technologies Program (www.eere.energy.gov/hydrogenandfuelcells).

[2] U.S. DOE Hydrogen Program, "National Hydrogen Energy Roadmap," Washington, DC, April 2002 (http://www1.eere.energy.gov/hydrogenandfuelcells/pdfs/national_h2_roadmap.pdf).

[3] *Hydrogen in Metals I*, Topics in Applied Physics, Vol. 28, edited by G. Alefeld and J. Völkl (Springer-Verlag, Heidelberg, 1978).

[4] Z. S. Wronski, Int. Mater. Rev. **46**, 1 (2001).

[5] L. Zaluski, A. Zaluska, P. Tessier, J. O. Ström-Olsen, and R. Schulz, J. Alloys Compd. **227**, 53 (1995).

[6] K. Yang, D. Chen, L. Chen, and Z. X. Guo, J. Alloys Compd. **333**, 184 (2002).

[7] C. X. Shang, M. Bououdina, Y. Song, and Z. X. Guo, Int. J. Hydrogen Energy **29**, 73 (2004).

[8] A. Zaluska, L. Zaluska, and J. O. Ström-Olsen, J. Alloys Compd. **298**, 125 (2000).

[9] L. Schlapbach and A. Zuttel, Nature (London) **414**, 353 (2001).

[10] A. C. Dillon and M. J. Heben, Appl. Phys. A: Mater. Sci. Process. **72**, 133 (2001).

[11] A. D. Lueking, R. T. Yang, N. M. Rodriguez, and R. T. K. Baker, Langmuir **20**, 714 (2004).

[12] A. Nikitin, H. Ogasawara, D. Mann, R. Denecke, Z. Zhang, H. Dai, K. Cho, and A. Nilsson, Phys. Rev. Lett. **95**, 225507 (2005).

[13] M. Ritschel, M. Uhlemann, O. Gutfleisch, A. Leonhardt, A. Graff, Ch. Täschner, and J. Fink, Appl. Phys. Lett. **80**, 2985 (2002).

[14] S. M. Lee and Y. H. Lee, Appl. Phys. Lett. **76**, 2877 (2000).

[15] J. S. Arellano, L. M. Molina, A. Rubio, and J. A. Alonso, J. Chem. Phys. **112**, 8114 (2000).

[16] Y. Okamoto and Y. Miyamoto, J. Phys. Chem. B **105**, 3470 (2001).

[17] G. Lu, H. Scudder, and N. Kioussis, Phys. Rev. B **68**, 205416 (2003).

[18] O. Gülseren, T. Yildirim, and S. Ciraci, Phys. Rev. Lett. **87**, 116802 (2001).

[19] T. Yildirim and S. Ciraci, Phys. Rev. Lett. **94**, 175501 (2005)..

[20] Y. F. Zhao, Y. H. Kim, A. C. Dillon, M. J. Heben, and S. B. Zhang, Phys. Rev. Lett. **94**, 155504 (2005).

[21] B. C. Pan, W. S. Yang, and J. Yang, Phys. Rev. B **62**, 12652 (2000).

[22] J. C. Charlier, T. W. Ebbesen, and Ph. Lambin, Phys. Rev. B **53**, 11108 (1996).

[23] P. M. Ajayan, V. Ravikumar, and J. C. Charlier, Phys. Rev. Lett. **81**, 1437 (1998).

[24] Y. Y. Xia, J. Z. H. Zhu, M. W. Zhao, F. Li, B. D. Huang, Y. J. Ji, X. D. Liu, Z. Y. Tan, C. Song, and Y. Y. Yin, Phys. Rev. B **71**, 075412 (2005).

[25] A. J. Lu and B. C. Pan, Phys. Rev. B **71**, 165416 (2005).

[26] H. F. Bettinger, J. Phys. Chem. B **109**, 6922 (2005).

[27] A. Hashimoto, K. Suenaga, A. Gloter, K. Urita, and S. Iijima, Nature (London) **430**, 870 (2004).

[28] G. Kresse and J. Furthmüller, Comput. Mater. Sci. **6**, 15 (1996).

[29] G. Kresse and J. Furthmüller, Phys. Rev. B **54**, 11169 (1996).

[30] D. Vanderbilt, Phys. Rev. B **41**, 7892 (1990).

[31] S. Logothetidis and C. Charitidis, Thin Solid Films **353**, 208 (1999).

[32] H. J. Monkhorst and J. D. Pack, Phys. Rev. B **13**, 5188 (1976).

[33] Y. Okamoto and Y. Miyamoto, J. Phys. Chem. B **105**, 3470 (2001).

[34] N. Jacobson, B. Tegner, E. Schroder, P. Hyldgaard, and B. I. Lundqvist, Comput. Mater. Sci. **24**, 273 (2002).

[35] G. Henkelman, B. P. Uberuaga, and H. Jónsson, J. Chem. Phys. **113**, 9901 (2000).

[36] P. O. Lehtinen, A. S. Foster, A. Ayuela, A. Krasheninnikov, K. Nordlund, and R. M. Nieminen, Phys. Rev. Lett. **91**, 017202 (2003).

[37] E. J. Duplock, M. Scheffler, and P. J. D. Lindan, Phys. Rev. Lett. **92**, 225502 (2004).

[38] J. A. Alonso, J. S. Arellano, L. M. Molina, A. Rubio, and M. J. López, IEEE Trans. Nanotechnol. **3**, 304 (2004).

[39] D. Y. Sun, J. W. Liu, X. G. Gong, and Zhi-Feng Liu, Phys. Rev. B **75**, 075424 (2007).

[40] A. J. Du and S. C. Smith, Nanotechnology **16**, 2118 (2005).

[41] G. Vidali, G. Ihm, H. Y. Kim, and M. W. Cole, Surf. Sci. Rep. **12**, 133 (1991).

[42] Y. Miura, H. Kasai, W. Diño, H. Nakanishi, and T. Sugimoto, J. Appl. Phys. **93**, 3395 (2003).

[43] E. Kaxiras and K. C. Pandey, Phys. Rev. Lett. **61**, 2693 (1988).

[44] P. A. Thrower and R. M. Mayer, Phys. Status Solidi A **47**, 11 (1978).

[45] K. Yamashita, M. Saito, and T. Oda, Jpn. J. Appl. Phys., Part 1 **45**, 6534 (2006).

[46] K. Kusakabe and M. Maruyama, Phys. Rev. B **67**, 092406 (2003).

[47] Y. Shibayama, H. Sato, T. Enoki, and M. Endo, Phys. Rev. Lett. **84**, 1744 (2000).
[48] O. E. Andersson, B. L. V. Prasad, H. Sato, T. Enoki, Y. Hishiyama, Y. Kaburagi, M. Yoshikawa, and S. Bandow, Phys. Rev. B **58**, 16387 (1998).
[49] Y. C. Ma, P. O. Lehtinen, A. S. Foster, and R. M. Nieminen, Phys. Rev. B **72**, 085451 (2005).
[50] O. L. Blakslee, D. G. Proctor, E. J. Seldin, G. B. Spence, and T. Weng, J. Appl. Phys. **41**, 3373 (1970).
[51] S. P. Chan, M. Ji, X. G. Gong, and Z. F. Liu, Phys. Rev. B **69**, 092101 (2004).
[52] H. Hemmes, A. Driessen, and R. Griessen, J. Phys. C **19**, 3571 (1986).